RESEARCH ARTICLE

NANO · MICRO small
www.small-journal.com

Large Language Model-Assisted Genotoxic Metal-Phenolic Nanoplatform for Osteosarcoma Therapy

Qingxin Fan, Yunxiang He, Jialing Liu, Qinling Liu, Yue Wu, Yuxing Chen, Qingyu Dou, Jing Shi, Qingquan Kong, Yunsheng Ou, and Junling Guo**

Osteosarcoma, a leading primary bone malignancy in children and adolescents, is associated with a poor prognosis and a low global fertility rate. A large language model-assisted phenolic network (LLMPN) platform is demonstrated that integrates the large language model (LLM) GPT-4 into the design of multifunctional metal-phenolic network materials. Fine-tuned GPT-4 identified gossypol as a phenolic compound with superior efficacy against osteosarcoma after evaluating across a library of 60 polyphenols based on the correlation between experimental anti-osteosarcoma activity and multiplexed chemical properties of polyphenols. Subsequently, gossypol is then self-assembled into Cu^{2+}-gossypol nanocomplexes with a hyaluronic acid surface modification (CuGOS NPs). CuGOS NPs has demonstrated the ability to induce genetic alterations and cell death in osteosarcoma cells, offering significant therapeutic benefits for primary osteosarcoma tumors and reducing metastasis without adverse effects on major organs or the genital system. This work presents an LLM-driven approach for engineering metal-organic nanoplatform and broadening applications by harnessing the capabilities of LLMs, thereby improving the feasibility and efficiency of research activities.

1. Introduction

Osteosarcoma is one of the most common primary bone malignancies, with almost half of all new cases occurring in children and young adults.[1] Almost all patients are considered to have subclinical micrometastases at the time of diagnosis, and the 3-year survival rate for patients with osteosarcoma who develop pulmonary metastases is only 30%.[2] Despite the never-ending research targeting therapeutic strategies for osteosarcoma, the overall prognosis for osteosarcoma has remained largely unchanged for over four decades.[2a] Therefore, the research for new therapeutic approaches for osteosarcoma is of great significance.

Natural polyphenols, ubiquitous in plants and other organisms, are promising versatile "green" building blocks for engineering multifunctional materials, owing to their diverse chemical and biological attributes.[3] These compounds have drawn

Q. Fan, Y. Chen, Y. Ou
Department of Orthopedics Surgery
The First Affiliated Hospital of Chongqing Medical University
Chongqing Medical University
Chongqing 400016, China
E-mail: junling.guo@scu.edu.cn

Q. Fan, Y. Chen, Y. Ou
Orthopaedic Research Laboratory of Chongqing Medical University
Chongqing Medical University
Chongqing 400016, China

Y. He, Y. Wu, J. Guo
BMI Center for Biomass Materials and Nanointerfaces, College of Biomass Science and Engineering
Sichuan University
Chengdu, Sichuan 610065, China
E-mail: junling.guo@ubc.ca

Y. He, Y. Wu, J. Guo
National Engineering Laboratory for Clean Technology of Leather Manufacture, Ministry of Education Key Laboratory of Leather Chemistry and Engineering
Sichuan University
Chengdu, Sichuan 610065, China

J. Liu
State Key Laboratory of Oral Diseases and National Clinical Research Center for Oral Diseases
West China Hospital of Stomatology
Sichuan University
Chengdu, Sichuan 610041, China

Q. Liu
Tea Refining and Innovation Key Laboratory of Sichuan Province, College of Horticulture
Sichuan Agricultural University
Chengdu, Sichuan 611130, China

Q. Dou
National Clinical Research Center for Geriatrics
Center of Gerontology and Geriatrics
West China Hospital
Sichuan University
Chengdu, Sichuan 610041, China

Q. Dou, Q. Kong
Department of Orthopedic Surgery and Orthopedic Research Institute
West China Hospital
Sichuan University
Chengdu, Sichuan 610041, China

The ORCID identification number(s) for the author(s) of this article can be found under https://doi.org/10.1002/smll.202403044

DOI: 10.1002/smll.202403044

substantial attention for their therapeutic potential in anti-inflammatory, antioxidant, and anti-tumor applications.[4] Notably, polyphenols such as quercetin, epigallocatechin gallate (EGCG), resveratrol, naringenin, tannic acid, and curcumin have shown significant activity against osteosarcoma.[5] However, the anti-tumor efficacy of these polyphenols is relatively modest, coupled with a narrow safety window, which limits their translation into clinical applications. Moreover, the manual experimental screening of a large library of natural polyphenols is often laborious and time-consuming, hindered by the need to assess the chemical and biological properties of polyphenols for both material development and clinical outcomes. Consequently, there is an urgent need to develop a cost-efficiency approach to develop a more potent and specific anti-osteosarcoma polyphenolic nanoplatform with enhanced therapeutic effectiveness.

With the rapid advancement of artificial intelligence (AI), its potential applications in drug discovery and screening have expanded tremendously.[6] While traditional AI has been instrumental in the evolution of drug screening, significant areas for improvement remain, such as poor natural language processing capabilities, limited contextual understanding, and great challenges in integrating multidisciplinary knowledge. These systems often require structured data inputs and face scalability issues, rendering them less efficient in the dynamic and complex field of therapy development. In contrast, advanced large language models (LLMs) like GPT-4 (OpenAI) represent a substantial leap forward. GPT-4′s proficiency in integrating information across disciplines and offering intuitive interfaces makes information more accessible. Moreover, its adaptability and capability for precise customization for therapeutic screening tasks enhance both scalability and operational efficiency.[7] This positions GPT-4 as an instrumental tool in overcoming the constraints of traditional AI, revolutionizing nanotherapeutic discovery and development processes.

Herein, we developed a large language model-assisted phenolic network (LLMPN) nanoplatform utilizing GPT-4 for the targeted screening of phenolic building blocks aimed at the inhibition of osteosarcoma progression. Specifically, GPT-4 offers cost-efficiency and seamless integration into existing experimental processes to generate the correlation between experimental anti-osteosarcoma activity and multiplexed molecular features of polyphenols. Then, multiple correlations indicated that gossypol might have excellent anti-osteosarcoma activity from a pool of 60 polyphenol candidates. In vitro experiments further confirmed the efficient inhibition ability of gossypol against osteosarcoma cells (**Figure 1**A–C). However, we found that the extremely poor water solubility of gossypol raised our concerns about its performance in clinical applications. Coordination between metal ions and polyphenols is a stable and straightforward strategy for nanomaterial self-assembly. Given considerations of metal valence, biological safety, and efficient yet unique mechanisms of cytotoxicity, we selected copper ions (Cu^{2+}) as the cation component in the metal-phenolic network (MPN), coordinating with the phenolic hydroxyl groups in gossypol to form assembled Cu^{2+}-gossypol nanocomplexes (Pre-CuGOS NPs).[8] Subsequently, the Pre-CuGOS NPs were surface-modified with hyaluronic acid (HA), thereby enhancing the stability and targeting of the nanoplatform (referred to as CuGOS NPs).[9]

We demonstrated that CuGOS NPs are preferentially internalized by osteosarcoma cells due to the enhanced retention effect and their interaction with HA-CD44. This cellular internalization leads to the release of gossypol and Cu^{2+} ions within the acidic lysosomal environment, effectively disrupting the genetic mechanisms of the osteosarcoma cells and leading to the genotoxic cell death (Figure 1D). In an orthotopic osteosarcoma model, CuGOS NPs showed remarkable therapeutic effects on primary osteosarcoma tumors and inhibition of metastasis with no adverse effects on main organs, including kidneys, lungs, genital system, and liver. This study not only demonstrates the integration of LLM into the design of new metal–organic nanoplatform, but also showcases the potential of AI for broadened biomedical applications, thereby significantly enhancing the practicality and efficiency of research initiatives.

2. Results and Discussion

2.1. Rational Prediction of Anti-Osteosarcoma Polyphenols

Nine structurally representative polyphenols were used to treat K7M2 cells to test their anti-osteosarcoma activity by cell counting kit-8 (CCK-8) assay (**Figure 2**A). GPT-4 was used as a foundational AI model to correlate with the half maximal inhibitory concentration (IC50) (Figure 2B). IUPAC name is a nomenclature that contains information about the basic molecular structure of chemical molecules. The IC50 values and IUPAC names were inputted to allow GPT-4 to self-tune and analyze the chemical features associated with the anti-osteosarcoma activity. The results of GPT-4 concluded that the IC50 values of the polyphenols were associated with the multiplexed properties of polyphenols, including chemical structures of Gallate Groups, Binding Affinity, Methoxy Groups, Solubility, Molecular Size and Shape, Phenyl Rings, Electronic Properties, Reactivity, Hydroxy Groups, Stability, and Chromen Structure Groups parameters. After adding the multi-dimensional values of these parameters, GPT-4 was further developed to perform linear correlation analysis between these parameter values and the corresponding IC50 values. The results showed that the IC50 values had strong negative correlations with solubility (XLogP3-AA value, $r = -0.571$), Hydroxy Groups (Phenolic Hydroxyl Number, $r = -0.538$), and Phenyl Rings (Benzene Ring Number, $r = -0.504$) (Figure 2C). The results of the correlation analysis between XLogP3-AA, Phenolic Hydroxyl Number, and Benzene Ring Number suggest that we can make a preliminary judgment on the polyphenol structure's

J. Shi, Q. Kong
Section of Science and Education
Hospital of Chengdu Office of People's Government of Tibetan Autonomous Region (Hospital.C.T.)
Chengdu, Sichuan 610041, China
J. Guo
State Key Laboratory of Polymer Materials Engineering
Sichuan University
Chengdu, Sichuan 610065, China
J. Guo
Departments of Chemical, Biological Engineering
The University of British Columbia
Vancouver, BC V6T1Z4, Canada

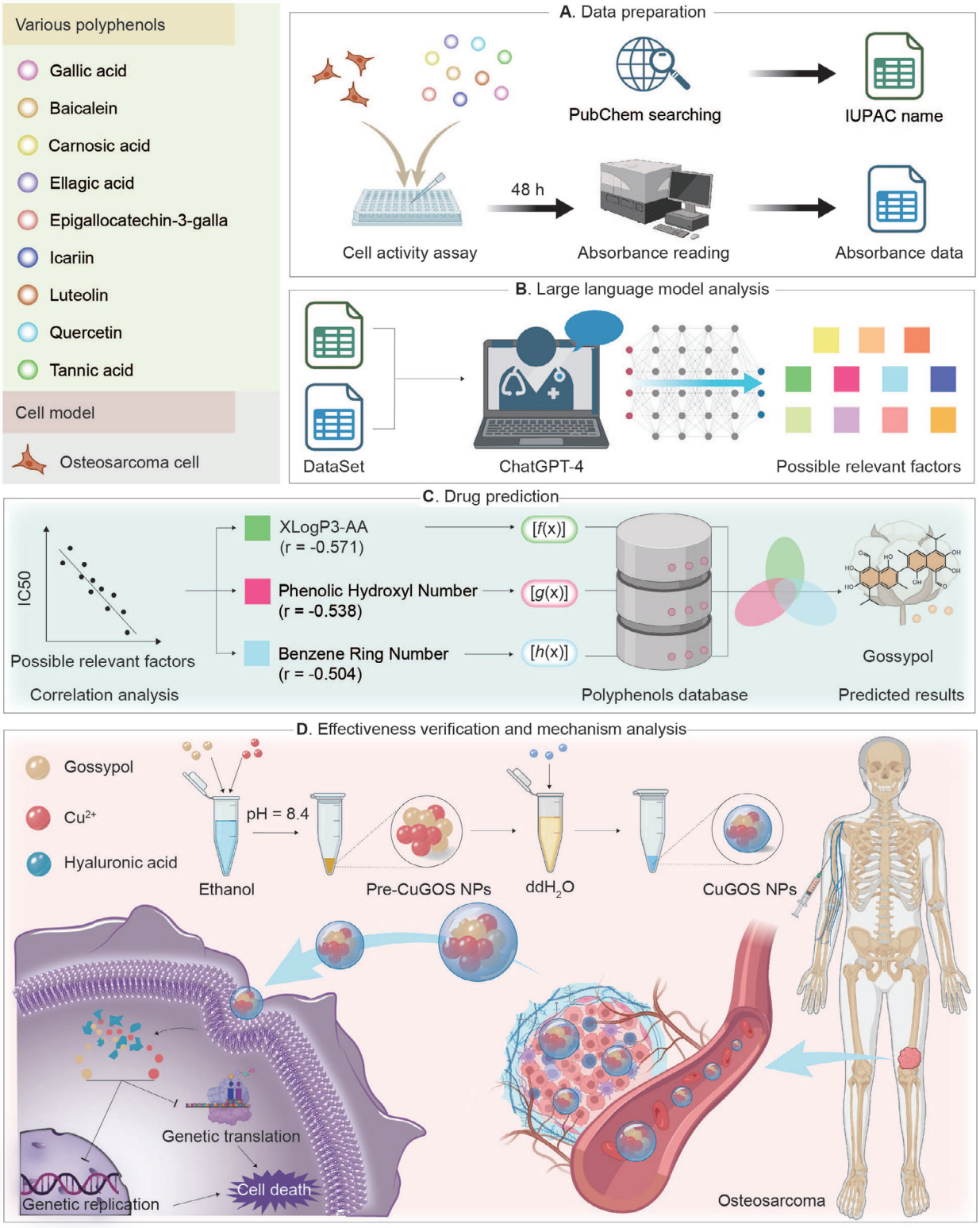

Figure 1. Schematic illustration of LLM-assisted screening of phenolic building blocks and engineering gossypol-based metal-phenolic nanoparticles (CuGOS NPs) for treating osteosarcoma. A) Obtained absorbance data of various polyphenol treated K7M2 cells and collected International Union of Pure and Applied Chemistry (IUPAC) name of various polyphenols. B) GPT-4 was used as an LLM model to find the correlation between anti-osteosarcoma activity and chemical feature. C) Validated correlations and built functions, predicted potential excellent anti-osteosarcoma activity of gossypol from polyphenol library using multiple functions. D) Construction of CuGOS NPs and validation of its anti-osteosarcoma effect and mechanism.

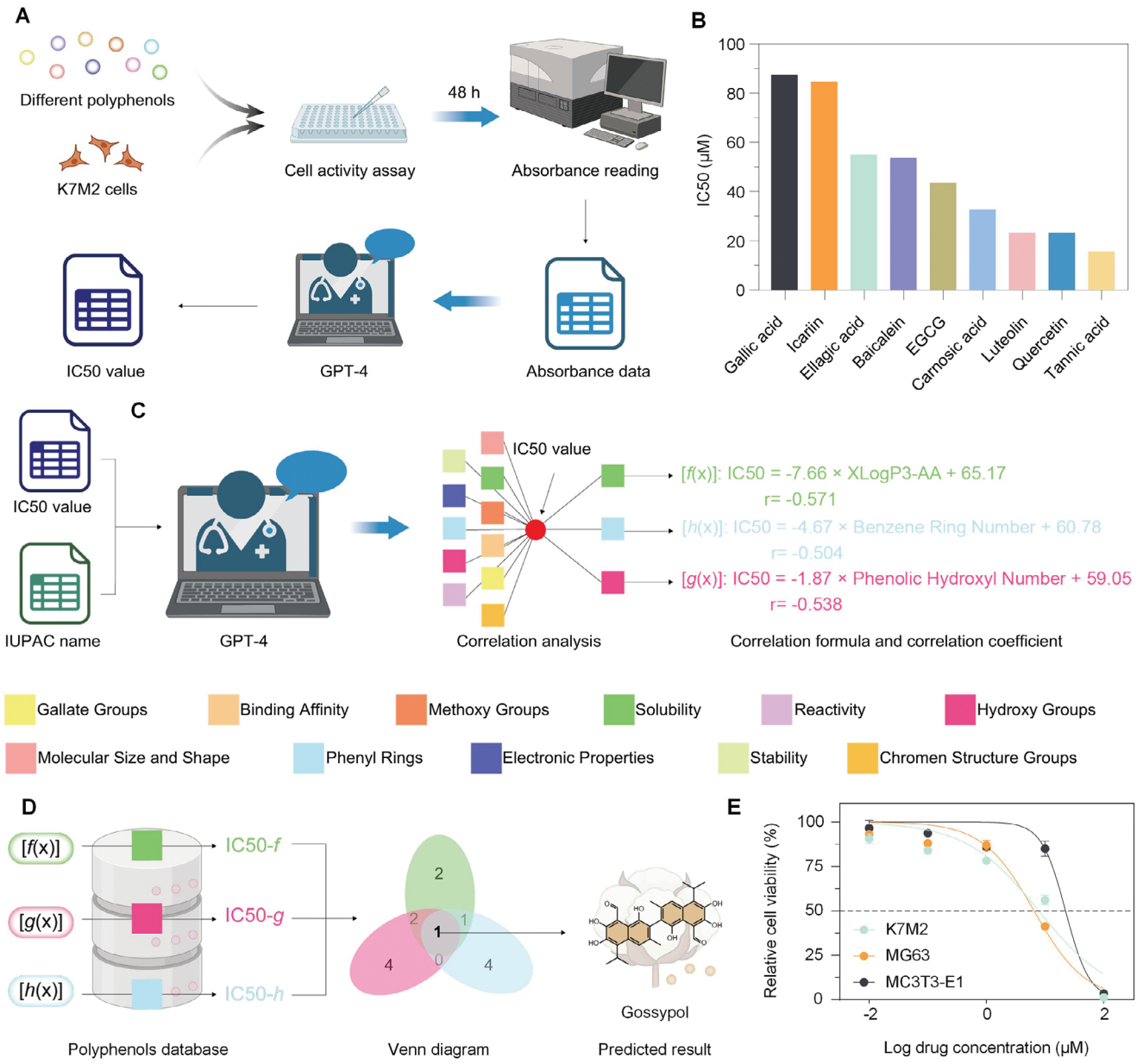

Figure 2. Fine tuning of GPT-4 and assisted screening process for anti-osteosarcoma based on a molecular pool of polyphenols. A) The IC50 values of various polyphenols to inhibit K7M2 cells were obtained by CCK-8 assay and GPT-4. B) The effect of various polyphenols on osteosarcoma cells was tested by CCK-8 assay ($n = 3$). The calculation method of IC50: 1) Averaging three independent inhibition rates; 2) Fitting the averaged inhibition rates for each concentration; 3) Calculating the IC50 value. C) GPT-4 was used to predict the possible relationship between the anti-osteosarcoma activity of polyphenols (IC50 value) and the chemical structure (IUPAC name) and to construct correlation functions. D) The IC50 values of the polyphenols in the library were calculated according to the correlation functions, and gossypol was filtered by the intersection of the results of multiple function calculations. E) Validation of anti-osteosarcoma activity of gossypol using K7M2, MG63, and MC3T3-E1 cells. Data were presented as mean ± SD ($n = 3$).

anti-osteosarcoma activity by analyzing the number of Benzene Ring Numbers in it (Figure S1A–C, Supporting Information).

Due to the absence of a dedicated polyphenol database, obtaining the structural parameters for polyphenols has proven to be quite challenging. We were able to gather data on only 60 polyphenols from over 10000 reports. For the remaining compounds, we conducted individual searches in PubChem and manually extracted the necessary structural parameters. The IC50 values of the polyphenols were further calculated using the correlation function formulae based on the XLogP3-AA value, the Phenolic Hydroxide Number, and the Benzene Ring Number. The polyphenols with the lowest IC50 values (10%) were selected as pooling elements. Ultimately, all three functions predicted that gossypol might have excellent anti-osteosarcoma activity (Figure 2D). Specifically, gossypol is a natural compound found in the cotton plant with favorable antiviral, antiparasitic, antioxidant, and anticancer activities.[10] However, the performance in anti-osteosarcoma activity has not been reported.

Interestingly, we determined the antitumor activity of gossypol using in vitro experiments, and the IC50 of gossypol was only 6.5 μM for MG63 cells and 7.7 μM for K7M2 cells. Notably, the IC50 of gossypol for the osteoblast cell line MC3T3-E1 was 22.4 μM, significantly higher than that of the osteosarcoma cells, suggested that gossypol has a specific inhibition effect (Figure 2E).

2.2. Fabrication and Characterization of CuGOS NPs

The water solubility of compounds plays a crucial role in the clinical translation. It can enhance the bioactive properties and the pharmacokinetic properties of compounds in vivo. In contrast, poor water solubility reduces the exposure of the compound and affects its efficacy.[11] In our studies, the extremely low water solubility of gossypol (XLogP3-AA value = 6.9) raises concerns about its clinical translation and bioavailability. Nanotechnology or nanoformulation provides significant impetus for efficient drug delivery of insoluble compounds.[12] Our group and others previously reported the MPN material platform, which are supramolecular materials consisting of metal ions and polyphenols.[8] MPN materials have been widely used in various fields due to their minimalist, rapid as well as versatility advantages.[13] In view of the outstanding performance of Cu^{2+} ions in the field of tumor therapy, we designed a self-assembled formation of MPN nanoparticles based on Cu^{2+} ions and gossypol with surface modification of HA, referred to as CuGOS NPs (**Figure 3**A). The nanosized gossypol-based MPN nanosystem significantly reduced the particle size to ≈142 nm and increased the homogeneity of particle size (Figure 3B). The modification of HA can increase the zeta potential of the nanoparticles (Figure 3C). Notably, the CuGOS NPs suspension did not show significant aggregation and precipitation even after three days. (Figure S2A, Supporting Information). In contrast, Pre-CuGOS NPs (without HA) showed significant precipitation after one day of standing at 4 °C (Figure S2B, Supporting Information). Dynamic light scattering detected that the size of Pre-CuGOS NPs increased, while the size of CuGOS NPs did not change significantly (Figure S2C, Supporting Information). It was suggested that the modification of HA significantly improved the stability of CuGOS NPs as HA is often used as a surface modification to enhance the stability of agent-delivery nano-carrier.[9,14] X-ray diffractograms (XRD) of CuGOS NPs did not show crystalline peaks, suggesting their amorphous substances (Figure 3D), the selected area electron diffraction (SAED) pattern result was further evidence the amorphous supmolecular structure as other MPN materials (Figure 3I). Energy dispersive spectroscopy (EDS) and X-ray photoelectron spectroscopy (XPS) were used to confirm the elemental composition of the CuGOS NPs. The XPS of the CuGOS NPs was calibrated with C1s at 284.8 eV, and the results showed the characteristic peak binding energies of Cu at 935 eV, O1s at 533 eV, and C1s at 285 eV (Figure 3E). To enhance the accuracy of SEM-EDS, we obtained the cluster of CuGOS NPs with relatively larger sizes as the research objects. The EDS results further confirmed the elemental compositions of Cu, C, and H in the CuGOS NPs (Figure S2D,E, Supporting Information). The morphology of CuGOS NPs was observed using scanning electron microscopy (SEM) and transmission electron microscopy (TEM). It could be observed that CuGOS NPs were irregularly spherical (Figure 3F,G). The HA layer around the CuGOS NPs was also observed on TEM images (Figure 3H). Using the UV absorption method, we calculated the loading rates of gossypol was 76.72% ± 0.51%, Cu^{2+} ions was 18.38% ± 0.12%, and HA was 4.89% ± 0.63% in CuGOS NPs.

2.3. Comprehensive Evaluation of CuGOS NPs Against Osteosarcoma

We investigated the hemolysis rate, uptake efficiency, and drug release property of CuGOS NPs. The hemolysis rate is an essential indicator for assessing the biosafety of intravenous drugs,[15] and thus we performed a hemolysis assay on CuGOS NPs. Since the color of CuGOS NPs interferes with the detection of absorbance, the water suspension of CuGOS NPs was used as a control. No significant hemolysis (< 5%) was observed when erythrocytes were co-incubated with 0–5 mg mL^{-1} of CuGOS NPs for 4 h (**Figure 4**A). This result suggested that therapeutic doses of CuGOS NPs did not have much effect on the hematologic system after intravenous administration.

To better understand the uptake efficiency of CuGOS NPs by osteosarcoma cells, we examined the intracellular fluorescence intensity after co-culturing Cy5-CuGOS NPs with K7M2 cells. According to previous reports, significant uptake of HA-modified nanoparticles could be observed within 8 h.[16] Here, we observed substantial intracellular enrichment of Cy5-CuGOS NPs after 4 h of co-incubation with cells (Figure 4B). After 6 h, the intracellular Cy5-CuGOS NPs decreased slightly and reached stability (Figure 4C). This may be related to exocytosis of tumor cells.[17] Confocal fluorescence microscopy further confirmed that the fluorescence was mainly derived from intracellular Cy5-CuGOS NPs. We found that osteosarcoma cells ingested with Cy5-CuGOS NPs were significantly swollen (Figure 4D). Considering that 4 h of uptake was not sufficient for the cleavage of Cy5-CuGOS NPs and that the surface modification of HA hindered the contact of the nano-active components with the signaling molecules on the cell surface, it is likely that it is related to the preference of osteosarcoma cells for Cy5-CuGOS NPs. The drug release profile was determined in PBS solution at 37 °C. After 72 h, the release rate of gossypol in PBS at pH = 5.5 was 87% ± 1.38%, which was significantly higher than its release rate at pH = 6.8 (26.38 ± 1.48%) and 7.4 (14.22 ± 1.67%) (Figure 4E). The fact that an acidic environment can significantly promote the cleavage of CuGOS NPs provides the basis for releasing gossypol with Cu^{2+} ions in tumor cells. The irradiation of violet (405 nm), green (532 nm), and red (640 nm) lasers promoted the release of drugs from CuGOS NPs, with green light showed the best release-promoting effect ($P < 0.001$). Heating can also significantly promote the release of drug from CuGOS NPs (Figure 4F).

2.4. In Vitro Anti-Osteosarcoma Ability of CuGOS NPs Based on Genotoxicity

The cytotoxicity of CuGOS NPs on osteosarcoma cells was investigated by CCK-8 assay. CuGOS NPs intervened in osteosarcoma cells for 24 h and showed an IC50 of 1.36 μM, significantly lower than that of gossypol only (6.6 μM) and considerably higher than that of Pre-CuGOS NPs (23.8 nM). CuGOS NPs

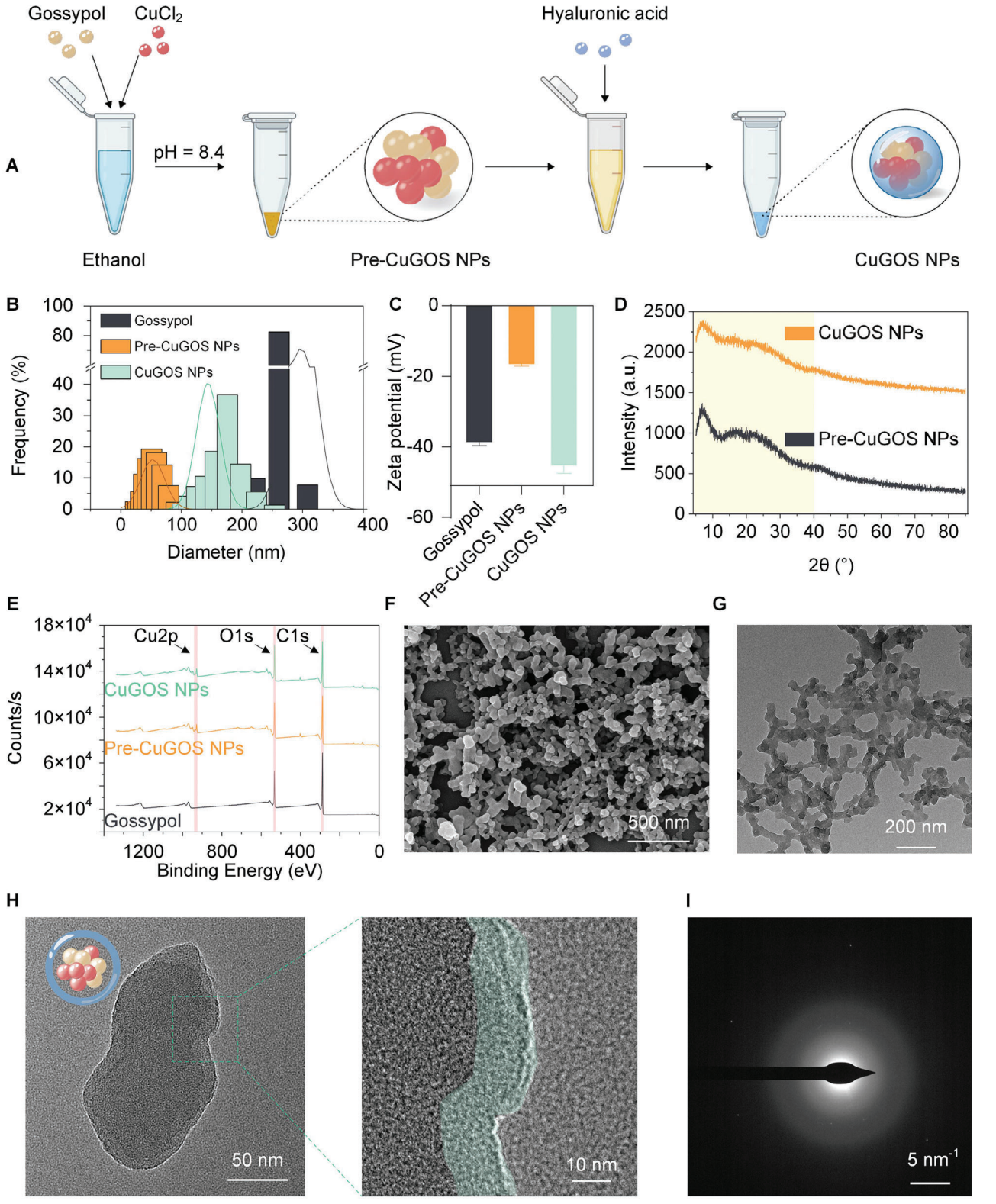

Figure 3. Synthesis and characterizations of CuGOS NPs. A) Schematic illustration of CuGOS NPs preparation: gossypol and $CuCl_2$ were wholly dissolved in ethanol solution at a molar ratio (1:1), adjusted the pH to 8.4, and vortexed rapidly. Pre-CuGOS NPs (without HA) were resuspended with ddH_2O, and CuGOS NPs were obtained after co-incubation of precipitation with HA in ddH_2O. B) Size distribution of CuGOS NPs. Data were presented as mean ± SD ($n = 3$). C) Zeta potential distribution of CuGOS NPs. Data were presented as mean ± SD ($n = 3$). D) XRD spectrum of CuGOS NPs. E) XPS of CuGOS NPs. F) SEM images, G,H) TEM images, and I) SAED images of CuGOS NPs.

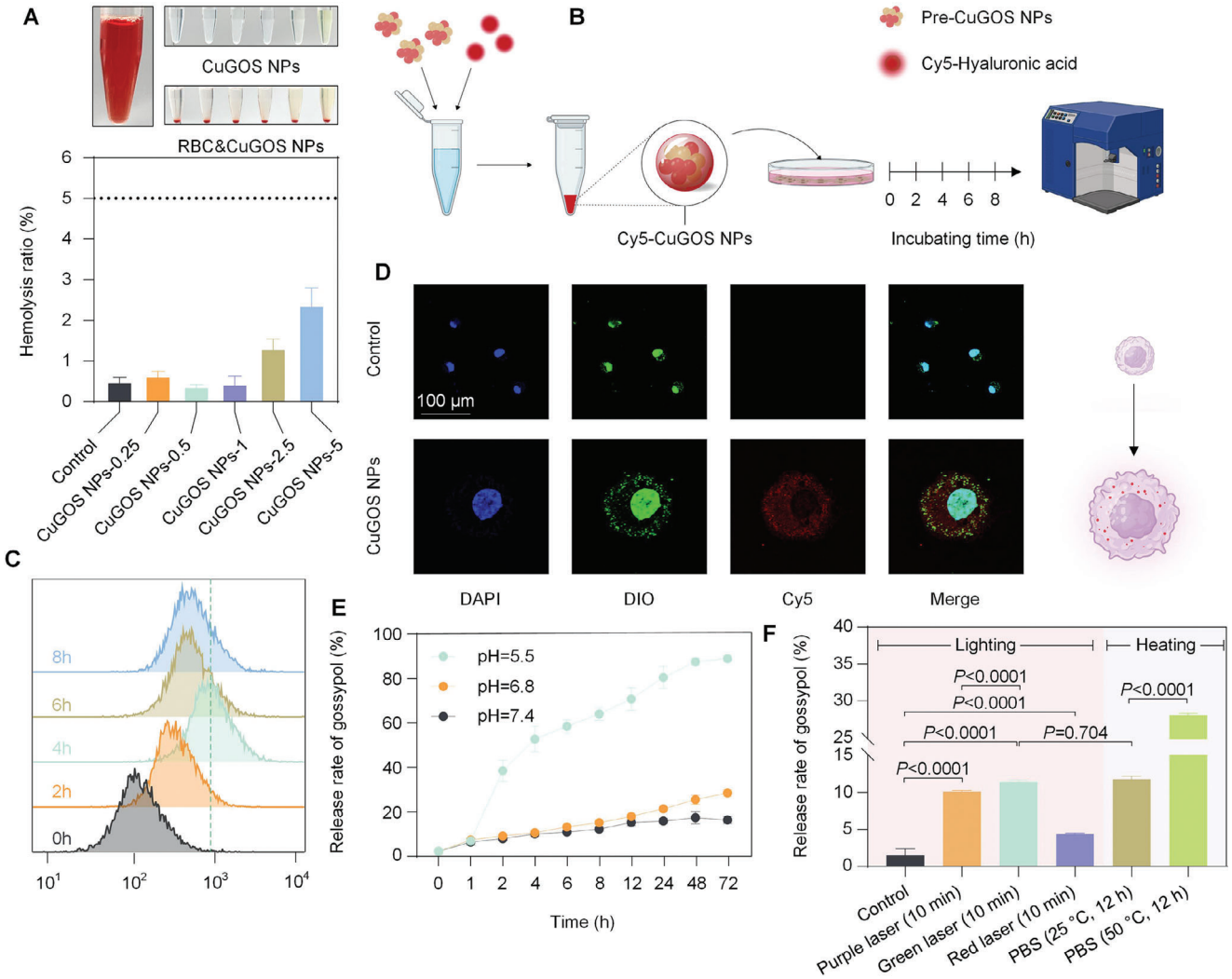

Figure 4. Hemolysis rate, uptake efficiency, and drug release of CuGOS NPs. A) Hemolysis assay on erythrocytes with different doses of CuGOS NPs. CuGOS NPs suspension was used as blank control, and lysed erythrocyte solution was used as positive control. Data were presented as mean ± SD (n = 3). B) Preparation of Cy5-CuGOS NPs and observation of uptake efficiency of K7M2 cells at different time points by flow cytometry. C) Flow cytometry observed Cy5-CuGOS NPs uptake by K7M2 cells at different times. D) Cy5-CuGOS NPs uptake by K7M2 cells at 4 h by confocal microscopy. Untreated K7M2 cells served as negative controls. E) Drug release curve of CuGOS NPs at pH 7.4, 6.8, and 5.5. Data were presented as mean ± SD (n = 3). F) Drug release curve of CuGOS NPs under different light (100 mW) and temperature conditions. Data were presented as mean ± SD (n = 6, one-way ANOVA).

intervened in osteosarcoma cells for 72 h and reached an IC50 of 20.27 nM, which was similar to the IC50 of Pre-CuGOS NPs (20.31 nM) (**Figure 5A**). In addition, we compared the toxicity of Pre-CuGOS NPs with other nine polyphenols-Cu^{2+} nano complexes (Figure S3A–I, Supporting Information) on osteosarcoma cells and found that Pre-CuGOS NPs exhibited the most excellent anti-osteosarcoma activity (Figure S3J, Supporting Information).

Based on referenced release curve (Figure 4E), CuGOS NPs may have a higher killing effect on osteosarcoma cells with increasing treatment time. The efficient uptake behavior is an essential advantage of CuGOS NPs in killing osteosarcoma cells. The CuGOS NPs were co-cultured with K7M2 cells for 4 h, and then the culture was continued after refreshing the medium. After 24 h, the IC50 value of CuGOS NPs was 4.07 μM, which was lower than that of Pre-CuGOS NPs (21.38 μM) and gossypol (185.1 μM) (Figure 5B). The results of apoptosis assays, scratch assays, clone formation, and transwell assays collectively supported that the internalized CuGOS NPs significantly increased apoptosis (Figure 5C; Figure S4, Supporting Information) and decreased migration (Figure 5D,E), clonal proliferation (Figure 5F), and invasion (Figure 5G–I) of K7M2 cells. These results suggested that CuGOS NPs could efficiently internalize by osteosarcoma cells and significantly inhibit their proliferation and migration. In addition, in vitro experiments revealed that CuGOS NPs significantly increased the sensitivity of osteosarcoma cells to doxorubicin (DOX, CI = 0.62) (Figure 5J). However, it is noteworthy that CuGOS NPs have significant antagonistic effects with cisplatin (CDDP, CI = 1.69), methotrexate (MTX, CI = 3.94), and especially ifosfamide (IFO, CI = 12.14) (Figure 5K–M).

To investigate the inhibition mechanism against osteosarcoma cells, transcriptome analysis was performed on K7M2 cells after the internalization of CuGOS NPs. Screening with

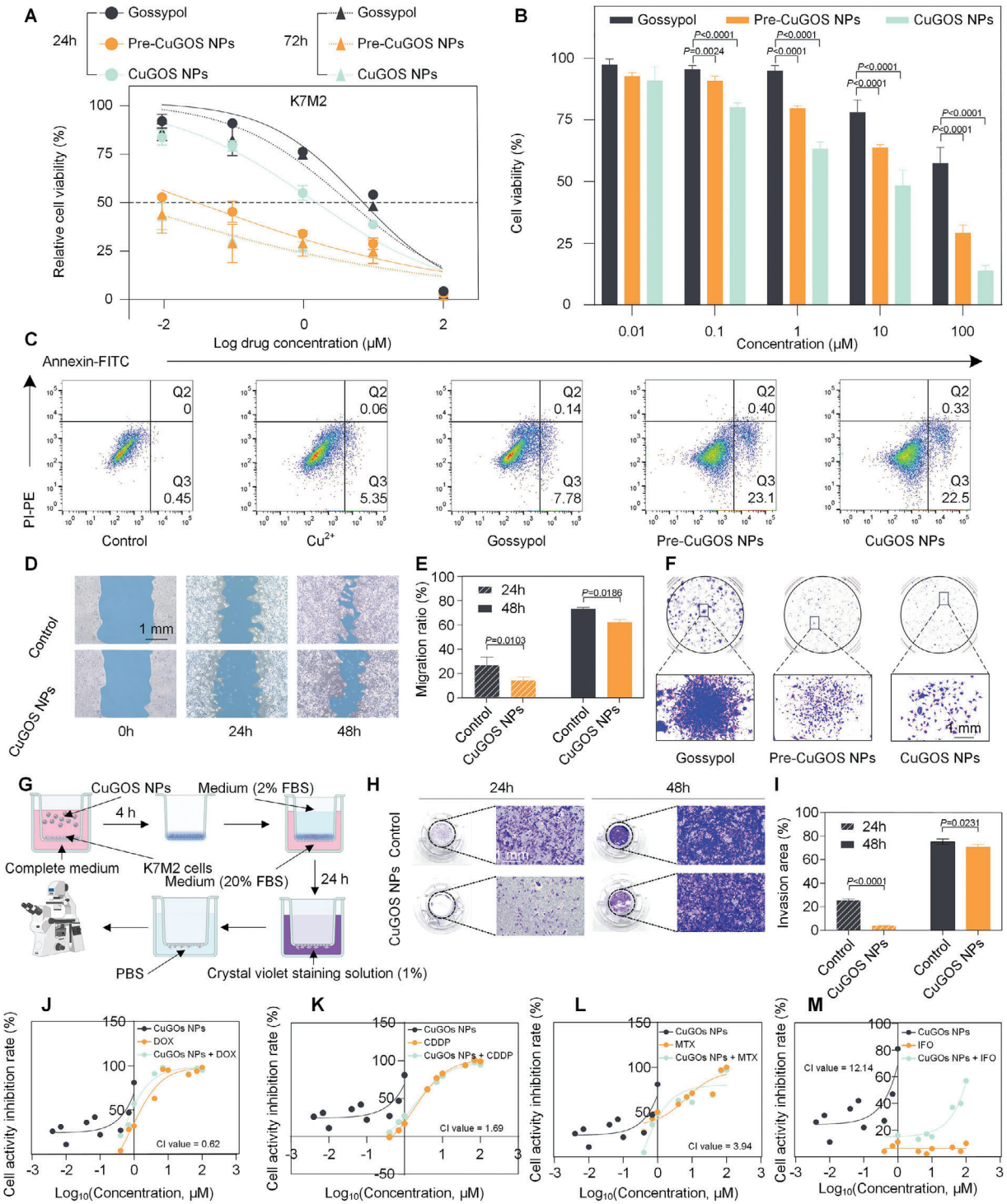

Figure 5. In vitro validation of the anti-osteosarcoma activity of CuGOS NPs. A) The cell viability of K7M2 cells after incubation with CuGOS NPs. Data were presented as mean ± SD ($n = 3$). B) The cell viability of K7M2 cells after incubation with internalized CuGOS NPs for 24 h. Data were presented as mean ± SD ($n = 3$, two-way ANOVA). C) Flow cytometric analysis of PI/Annexin V stained K7M2 cells to detect apoptosis following internalized Cu^{2+} ions, gossypol, Pre-CuGOS NPs, and CuGOS NPs stimulation for 24 h. D) Wound healing assay were used to evaluate the migration abilities of K7M2 cells. E) Quantitative analysis of K7M2 cells migration ratio. Data were presented as mean ± SD ($n = 3$, two-way ANOVA). F) Clone formation assay of K7M2 incubated with internalized gossypol, Pre-CuGOS NPs, and CuGOS NPs. G) Schematic illustration of the invasion experiments, fully internalized CuGOS NPs were used to in this experiment. H) Transwell assay was used to evaluate the invasion abilities of K7M2 cells. I) Quantitative analysis of K7M2 cells invasion ratio. Data were presented as mean ± SD ($n = 3$, two-way ANOVA). Effect of CuGOS NPs plus DOX J), CDDP K), MTX L), or IFO M) combinatorial treatment on the growth of osteosarcoma cell lines K7M2. Results from one representative experiment of 3 independent experiments are shown.

a threshold of $P < 0.05$ and $|\log_2(\text{Fold Change})| > 1$, 175 genes were found to be up-regulated and 187 genes were found to be down-regulated (Figure S5, Supporting Information). We flagged the 10 most significantly up-regulated and 10 most significantly down-regulated genes for tagging and searching. However, no studies related to these genes in osteosarcoma were found. For example, Sypnr,[18] Asb12,[19] and Ppp1r16b[20] is associated with the development of nerve. PDE6[21] and Frmd7[22] is associated with visual system development (**Figure 6A**). To minimize missing information, we selected the 20 genes with the smallest P-values to study and found that a decrease in Khdrbs3 was of interest (Figure 6B). KHDRBS3 increases blood-tumor barrier permeability, which enhances greater enrichment of drugs in tumor tissues.[23] Knockdown of KHDRBS3 promotes CD44v expression,[24] which can facilitate the internalization of HA-modified nanoplatforms.[25] Overexpressing KHDRBS3 increases tumor resistance by increasing glycolysis.[26] However, the role of KHDRBS3 in osteosarcoma progression remains to be further explored.

Gene ontology enrichment analysis showed that CuGOS NPs induced genetic alterations were significantly enriched in sperm motility and cilium movement, and this alteration was mainly derived from gossypol.[27] In molecular function classification, altered genes were significantly enriched in apoptosis and signaling (Figure S6, Supporting Information). Combined with previous experiments (Figure 5C; Figure S4, Supporting Information) and the reported studies, we hypothesized that this is a result of the synergistic effect of gossypol[28] and Cu^{2+} ions.[29] Kyoto Encyclopedia of Genes and Genomes (KEGG) analysis allowed us to note that many of the changed genes were significantly associated with genetic information processing, such as translation, transcription and folding, sorting, and degradation (Figure 6C). Gene Set Enrichment Analysis (GSEA) showed that 9 of the 10 gene sets with the lowest enrichment scores were strongly associated with genetic behavior, in descending order of enrichment score are ribosome, DNA replication, spliceosome, ribosome biogenesis, cell cycle, nucleocytoplasmic transport, mismatch repair, homologous recombination, and nucleotide excision repair (Figure 6D). Downregulation of these gene sets suggested that significant trauma to the genetic behavior of osteosarcoma cells, demonstrating the robust genotoxicity of CuGOS NPs. In addition, GSEA also revealed that apoptosis, necroptosis, mitophagy, ferroptosis, and autophagy related genes were significantly upregulated, suggesting that CuGOS NPs induce osteosarcoma cell death in multiple ways (Figure 6E). Whereas, the CuGOS NPs did not seem to affect the expression of osteosarcoma-causing genes (Myc and Ras) (Figure S7A–D, Supporting Information).

Genomic integrity is critical for the survival of an organism, and genotoxic therapy is an important approach for tumor treatment.[30] Genotoxic drugs cause extensive DNA damage by interfering with DNA replication and repair, ultimately leading to cell death.[31] The mechanism of anti-osteosarcoma of CuGOS NPs is like that of genotoxic drugs such as cyclophosphamide and cisplatin in that it induces tumor cell death by initiating genotoxic stress.[32] Unlike these drugs, CuGOS NPs not only inhibit the synthesis of genetic material, but also inhibit DNA damage repair in tumor cells, which is essential to enhance the sensitivity of tumor cells to genotoxic therapies.[33]

2.5. In Vivo Targeting and Biological Distribution

For genotoxic drugs, excellent targeting contributes to enhancing anti-tumor efficacy and is crucial for biosafety.[34] Therefore, after validating the anti-tumor effect and mechanism of CuGOS NPs in vitro, the in vivo fate was studied in the K7M2-derived orthotopic osteosarcoma model. Cy5-conjugated HA was utilized for the visualization of CuGOS NPs. In vivo, fluorescence imaging was used to analyze the distribution of CuGOS NPs in tumor and organs (Figure S8A, Supporting Information). The fluorescence intensity at the tumor peaked 24 h after intravenous injection. As the time gradually increased, the fluorescence intensity gradually shrank (Figure S8B, Supporting Information). Fluorescence imaging of the isolated tumor showed that clear fluorescent signals were still present 72 h after injection. These results demonstrated the tumor targeting and accumulation ability of CuGOS NPs. In addition, in vivo fluorescence imaging results showed that faint fluorescence was still present in the liver, testes, and lungs at 72 h after injection (Figure S8C,D, Supporting Information). Therefore, the effects of CuGOS NPs on these organs became the focus of our safety studies.

Inductively coupled plasma mass spectrometry analysis found that the Cu content was still abundantly enriched in tumor tissues within 72 h of injection. The Cu content in these organs decreased to different degrees, and only the liver ($P = 0.0005$) and lung ($P = 0.0042$) showed higher Cu content than the control group after 72 h of injection (Figure S9, Supporting Information).

2.6. In Vivo Antitumor Effects of CuGOS NPs Against Orthotopic Osteosarcoma

The therapeutic efficacy of CuGOS NPs was explored in the model of orthotopic osteosarcoma, in which CuGOS NPs were administrated every three days and the details protocol was shown in **Figure 7A**. After 14 days of intervention, the body weight of CuGOS NPs-treated mice group bearing osteosarcoma increased to 24.66 ± 0.49 g, which is significantly higher than that of control mice (22.08 ± 0.54 g) (Figure S11A, Supporting Information). Meanwhile, the CuGOS NPs significantly reduced the tumor volume when compared with other treatment or control groups (Figure 7B; Figure S11B, Supporting Information). In addition, the final tumor volume (Figure 7C) and weight (Figure 7D) were much lower in the CuGOS NPs-treated group, indicating that tumor growth was significantly inhibited. The degree of lesion shrinkage is an essential indicator for assessing the effectiveness of a tumor treatment regimen.[35] Immunohistochemical results of osteosarcoma tissues from the CuGOS NPs group showed a significant decrease in the expression of genetically behavioral representative genes (Rps3, Mcm2, Cdk1, Mlh1, Nbs1, Pold3) compared to the control group, which agrees with the results obtained from the transcriptome sequencing (Figure 7E; Figures S10–S12, Supporting Information). These in vivo and in vitro results further target the mechanism of CuGOS NPs' damage to osteosarcoma at the behavioral DNA damage. Besides, immunofluorescence showed more cytotoxic T-lymphocyte infiltration at the margins of osteosarcoma tissues in the CuGOS NPs group (Figure 7F), indicating that the immune microenvironment of osteosarcoma tissues was improved.

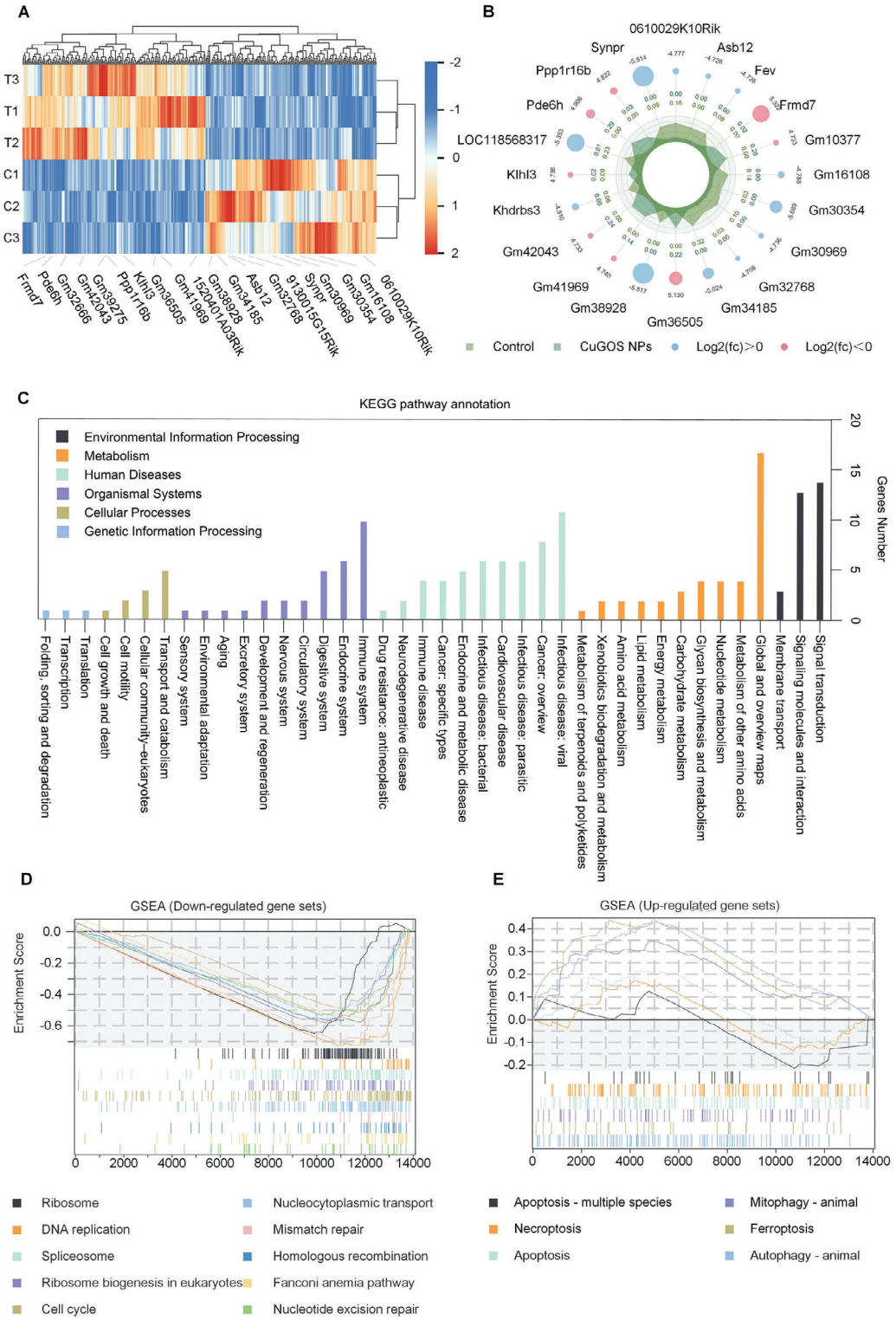

Figure 6. CuGOS NPs inhibit osteosarcoma cells through genotoxicity. A) Heatmap representation of differentially expressed genes, the 10 most significantly up-regulated genes, and the 10 most significantly down-regulated genes are labeled. B) Radar plot showing the 20 differentially expressed genes with the smallest p-values. First circle: up-regulated genes (light red) and down-regulated genes (light blue), the size of the circle varies according to the size of $\log_2$(Fold Change) value. Second circle: the data in the outer circle represents the average expression of the experimental group, and the data in the inner circle stands for the average expression of the control group. Third circle: visualization of the average expression of the genes in the two groups. C) KEGG pathway terms of differentially expressed genes between internalized CuGOS NPs treated and the control K7M2 cells. D) The 10 GSEA enrichment pathways with the lowest enrichment scores. E) GSEA of gene expression events up-regulated by CuGOS NPs.

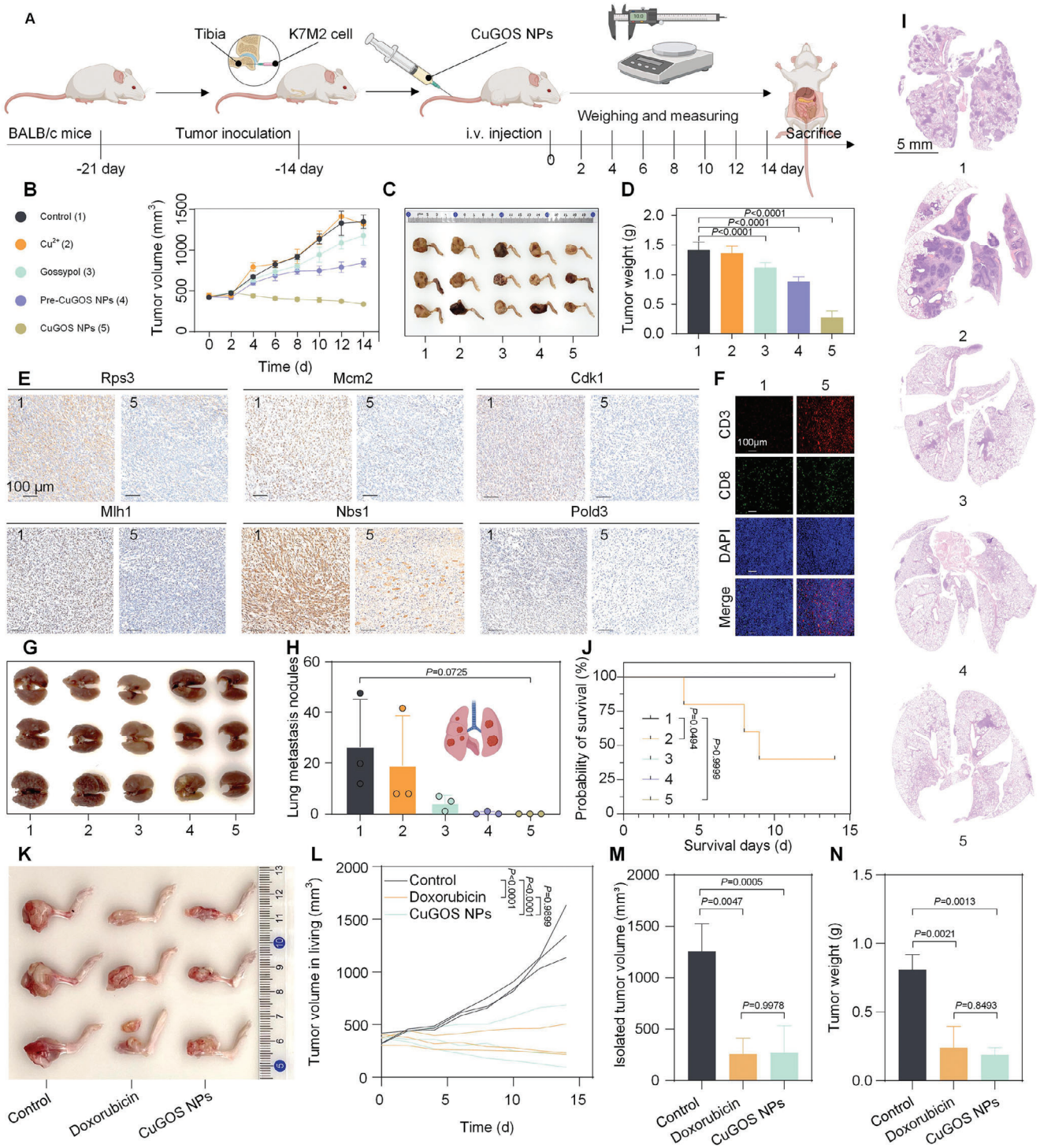

Figure 7. In vivo therapeutic effects of CuGOS NPs for inhibition of osteosarcoma growth and metastasis. A) Schematic illustration of the in vivo therapeutic schedule. B) Growth curves of orthotopic osteosarcoma with various treatments. Data were presented as mean ± SD ($n = 3$). C) Macroscopic photographs of the excised tumors at 14 days ($n = 3$). D) Average weights of excised tumors at observation endpoints. Data were presented as mean ± SD ($n = 3$, one-way ANOVA). E) The protein level of Rps3, Mcm2, Cdk1, Mlh1, Nbs1, and Pold3 in K7M2 primary tumor tissue were detected using immunohistochemistry staining. F) Representative images of protein expression of CD3 (red) and CD8 (green) in osteosarcoma tissue with immunofluorescence staining. G) Images of whole metastasis-bearing lungs. H) Counting of pulmonary metastatic nodules. Data were presented as mean ± SD ($n = 3$, one-way ANOVA). I) Representative histological sections of lungs with various treatments. J) Kaplan-Meier survival curve of tumor-bearing mice in each group ($n = 5$, log-rank test). K) Macroscopic photographs of the excised tumors at 14 days after treated with doxorubicin or CuGOS NPs ($n = 3$). L) Growth curves of orthotopic osteosarcoma treated with doxorubicin or CuGOS NPs ($n = 3$, two-way ANOVA). Average volume M) and weight N) of isolated tumors at observation endpoints. Data were presented as mean ± SD ($n = 3$, one-way ANOVA).

Distant metastases in almost all osteosarcoma patients often precede the onset of symptoms and are a significant cause of prognosis.[36] The lung is the most common site of distant metastasis for osteosarcoma.[1] We dissected lungs to assess the efficacy of CuGOS NPs in inhibiting lung osteosarcoma metastases. Significant metastatic lesions could be observed in the lungs of the control, Cu^{2+} ions-, and gossypol-treated groups, whereas few significant metastatic lesions could be detected in the CuGOS NPs-treated group (Figure 7G,H), and the lung weights were also significantly lower in the comparisons (Figure S11C, Supporting Information). Consistent with the direct observation, in histological examination of lung tissues, metastatic lesions were widely detected in the control, Cu^{2+} ions-, and gossypol-treated groups. Still, fewer metastatic lesions were observed in the CuGOS NPs-treated group, further supporting that CuGOS NPs could effectively inhibit distant osteosarcoma metastasis (Figure 7I). In vivo results showed that there was no significant difference in the anti-osteosarcoma effects of doxorubicin and CuGOS NPs (Figure 7K–N). Compared to the worrisome toxicity of doxorubicin, CuGOS NPs are more advantageous regarding safety.

2.7. In Vivo Biosafety and Biocompatibility of CuGOS NPs

The biosafety of the CuGOS NPs was further investigated in vivo. After 14 days of treatment, the mortality of the Cu^{2+} ions-treated group was high, reaching 70% (Figure 7J). We also noticed a significant increase in kidney weight (**Figure** 8A) and volume (Figure S13A, Supporting Information) in the gossypol- and Pre-CuGOS NPs-treated groups. In addition, the kidneys showed white ischemic areas (Figure 8B), accompanied by elevated blood urea nitrogen (BUN) (Figure S13B, Supporting Information) and creatinine (Cre) (Figure S13C, Supporting Information). Histological analysis showed abnormal renal tissue structure in gossypol- and Pre-CuGOS NPs-treated groups, with many tubular patterns, epithelial cells atrophy, neutrophil infiltration in the mesenchyme, and unclear glomerular and capillary collaterals. In contrast, the CuGOS NPs group did not show significant abnormalities in kidney-related indices (Figure 8C). These results suggested that the surface functionalization of HA can significantly ameliorate the nephrotoxicity of CuGOS NPs, which might be related to the enhancement of therapeutic performance.

The adverse side effects on main organs were also studied. In addition to the tumor metastases, the lungs of the Cu^{2+} ions-treated group showed many neutrophils and crystals, accompanied by severe pulmonary edema (Figure 8D). This suggested that direct intravenous injection of Cu^{2+} ions led to severe pneumonia. Then, the size of testes, vas deferens, and seminal glands in the Cu^{2+} ions group was also significantly smaller than those in the other groups (Figure 8E). Histological analysis of the testes showed structural abnormalities in the outer seminiferous tubules, with spermatogonia and spermatocytes reduced (Figure 8F). Moreover, gossypol, as a male contraceptive, had no significant effect on the reproductive system but has a great impact on the liver.[27] In the gossypol-treated group, serum alanine transaminase (ALT) was significantly higher than those in other groups (Figure S13D, Supporting Information), and serum aspartate aminotransferase (AST) also tended to be elevated (Figure S13E, Supporting Information). Histological analysis showed extensive hepatocyte edema with sparse cytoplasm vacuolization and neutrophilic infiltration. Finally, no obvious abnormality of main organs was observed in CuGOS NPs-treated group, including lung, testis, liver, heart, and spleen (Figure 8D–G; Figure S13, Supporting Information).

In the evaluation of ecological footprint, the lethal concentration half of CuGOS NPs for zebrafish (48 h) more than 100 mg L^{-1}, which is low or non-toxic to the water column (Figure 8H,I). The seed of pak choi mixed with CuGOS NPs had a higher germination rate (Figure 8J) and insect resistance (Figure 8K,L), and did not affect its growth (Figure 8M–O). Therefore, in general, the effects of CuGOS NPs on the ecological footprint are relatively safe and can even exert beneficial effects under certain conditions.

3. Conclusion

We established a promising LLMPN nanoplatform in the combination of advanced multi-modal capabilities of LLM with the flexible design capabilities of MPN materials. OpenAI GPT-4 was used to screen a comprehensive library of 60 phenolic candidates, identifying gossypol based on its correlation with anti-osteosarcoma activity and multidimensional chemical properties. GPT-4, fine-tuned for this specific task, pinpointed gossypol as a promising component exhibiting potent anti-osteosarcoma potential. This result is largely based on the characteristics of gossypol, specifically its high XLogP3-AA value, phenolic hydroxyl number, and number of benzene rings. Therefore, focusing on polyphenols with similar properties in future research could be instrumental in the discovery of novel anti-osteosarcoma drugs. The selective inhibition effect of gossypol on osteosarcoma cells was initially validated through in vitro assays. Subsequently, its bioavailability was significantly enhanced by forming CuGOS NPs, a self-assembled supramolecular MPN nanoplatform comprising gossypol and Cu^{2+} ions. Notably, osteosarcoma cells demonstrated a high uptake of CuGOS NPs, which were effective in disrupting genetic mechanisms and inhibiting tumor growth. However, the specific synergistic mechanism of gossypol with Cu^{2+} ions need to be excavated by comparing it with the mechanism exhibited by gossypol or copper treatment alone. In vivo studies further confirmed that CuGOS NPs markedly suppressed osteosarcoma tumor progression and lung metastasis, without inducing significant toxicities in the liver and kidneys. Overall, this research illustrates the power of an LLM-driven strategy in the development of metal–organic supramolecular systems, leveraging LLM capabilities to improve anti-tumor efficacy and expand the scope of applications, ultimately enhancing the practicality and efficiency of scientific investigations.

4. Experimental Section

Materials: HA (MW 10 kDa) was purchased from Bidepharm (Shanghai, China). Gossypol and other polyphenols were purchased from Rhawn (Shanghai, China). Dulbecco's Modified Eagle's Medium (DMEM) and Pancreatin were purchased from Gibico (New York, USA). Cyanine-5 labeled hyaluronic acid (MW = 10 kDa) was purchased from Yusi Medical Technology Co., Ltd. (Chongqing, China). Fetal bovine serum was ordered from ExCell Bio (Shanghai, China). Crystal violet ammonium oxalate solution, Paraformaldehyde, and Annexin V-FITC apoptosis

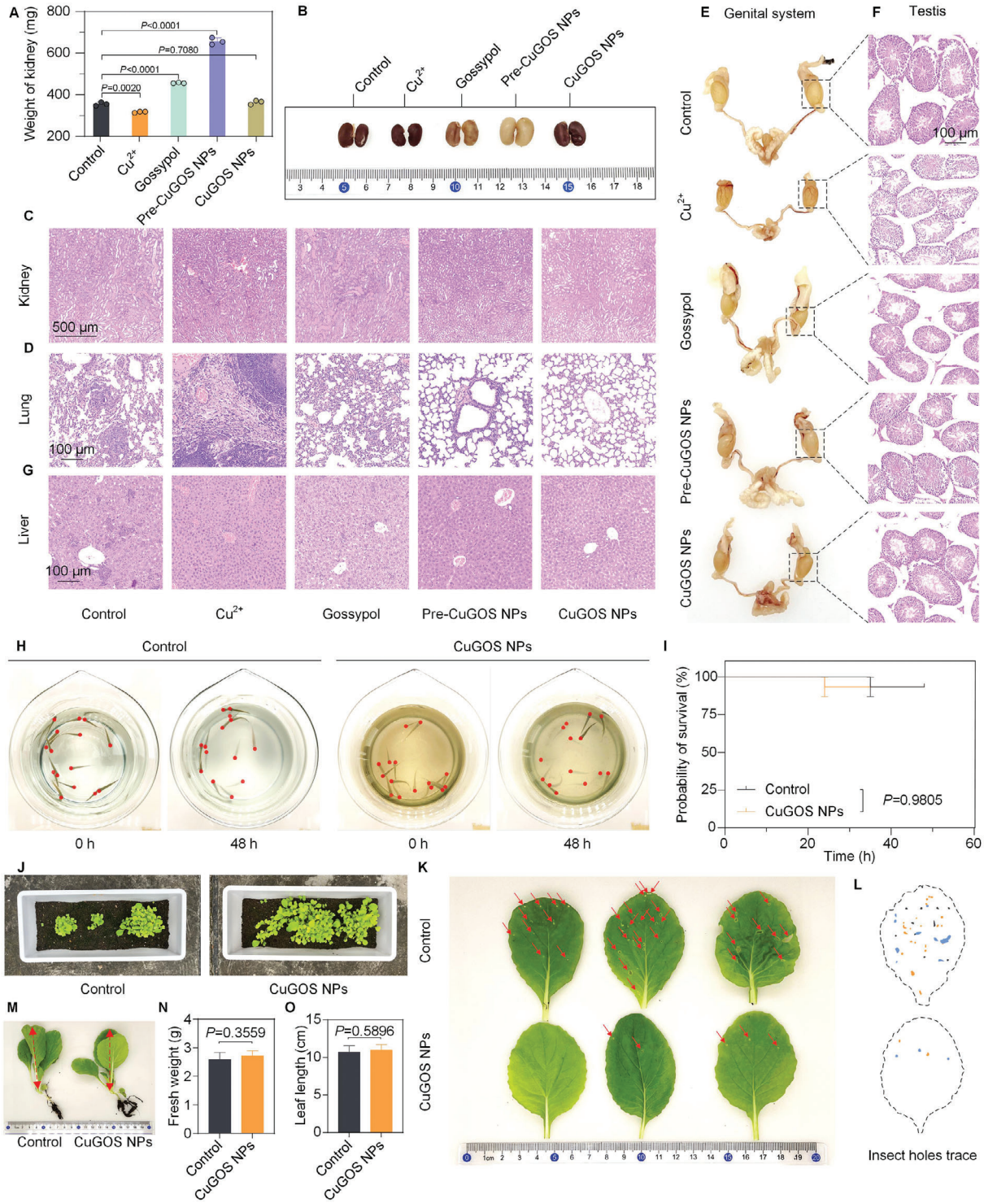

Figure 8. In vivo biocompatibility evaluation of CuGOS NPs. A) Average weights of kidneys at observation endpoints. Data were presented as mean ± SD ($n = 3$). B) Images of whole kidneys of each group. Representative histological sections of C) kidneys, D) lungs, F) genital system, and G) liver with various treatments. E) Images of the whole genital system of each group. H) Counts of zebrafish (red dots) in both groups after 48 h of treatment. Since the water in the CuGOS NPs group at 48 h was too turbid, we replaced 2/3 of the original water with fresh water before taking the photos to more clearly observe the number of zebrafish in this group. I) Kaplan-Meier survival curve of zebrafish in each group ($n = 15$, log-rank test). J) Observations on the germination rate of two groups two weeks after sowing. K) Number of insect holes (red arrows) on representative leaves four weeks after sowing. L) Traces of insect holes of two groups. M) Phenotypic images of representative pak choi of two groups four weeks after sowing. N) Average fresh weights of pak choi after treatment with CuGOS NPs for four weeks ($n = 5$, t-test). O) Average leaf lengths of pak choi after treatment with CuGOS NPs for four weeks ($n = 5$, t-test).

detection kit were purchased from Solarbio (Chengdu, China). $CuBr_2$, $CuSO_4$, and $CuCl_2$ were purchased from Adamas (Chengdu, China). Isoflurane was purchased from RWD (Shenzhen, China). DAPI and DIO were purchased from Biyuntian (Shanghai, China). Ribosomal protein S3 (Rps3), Minichromosome maintenance complex component 2 (Mcm2), Cyclin dependent kinase 1 (Cdk1), MutL homolog 1 (Mlh1), Nibrin (Nbs1), DNA polymerase delta 3 (Pold3), Small nuclear ribonucleoprotein U5 subunit 200 (SNRNP200), and nucleoporin 62 (NUP62) primary antibodies were purchased from Servicebio Biotechnology Co., Ltd. Other critical chemicals, if not specified, were described in the corresponding section. Balb/c mice (female, 5–6 weeks) were purchased from Dashuo Biotech (Chengdu, China). All Animal experiments have been approved by the Ethics Committee of the First Affiliated Hospital of Chongqing Medical University (No. 2022-K380) and meet the requirements of animal ethics and welfare.

Synthesis of CuGOS NPs and Other Pre-CuX NPs: The CuGOS NPs were synthesized using a self-assembly method based on the metal-phenolic network. Gossypol and $CuCl_2$-$2H_2O$ (molar ratio 2:2.5) were fully dissolved in absolute ethanol. Then, the solution pH was quickly adjusted to 8.4 with tris aqueous solution (10 mM, pH = 10.4) under vigorous stirring at 45 °C. The mixture was stirred for eight hours and centrifuged (13000 rpm, 10 min) to obtain the crude Pre-CuGOS NPs (without HA). The crude Pre-CuGOS NPs were washed with 10% ethanol and centrifuged to obtain high-purity Pre-CuGOS NPs. The Pre-CuGOS NPs were added to the hyaluronic acid solution (0.1 mg mL^{-1}, MW = 10 kDa) and stirred at room temperature for 24 h. Precipitation was collected by centrifugation, which was washed with ddH_2O to obtain CuGOS NPs. The synthesized Pre-CuGOS NPs and CuGOS NPs were freeze-dried and stored at 4 °C for spare parts.

Referring to the synthesis method of Pre-CuGOS NPs, nine other polyphenol complexes with Cu^{2+} ions (Pre-CuX NPs) were prepared. The complexes of baicalein with Cu^{2+} ions were named Pre-CuBAI NPs, the complexes of ellagic acid with Cu^{2+} ions were named Pre-CuELA NPs, the complexes of epigallocatechin gallate with Cu^{2+} ions were named Pre-CuEGCG NPs, the complexes of icariin complex with Cu^{2+} ions was named Pre-CuICA NPs, the complexes of luteolin complex with Cu^{2+} ions was named Pre-CuLUT NPs, the complexes of quercetin with Cu^{2+} ions was named Pre-CuQUE NPs, the complexes of tannic acid with Cu^{2+} ions were named Pre-CuTAN NPs, the complexes of gallic acid with Cu^{2+} ions were named Pre-CuGAA NPs, and the complexes of carnosic acid with Cu^{2+} ions were named Pre-CuCAR NPs.

In Vivo Tumor-Targeting and Bio-Distribution of the CuGOS NPs: Osteosarcoma mouse models were induced by K7M2[24], and Cy5-CuGOS NPs were administered to mice at a gossypol concentration of 20 mg kg^{-1}. Then, 1, 4, 8, 24, 48, and 72 h after intravenous injection, the images of mice were obtained using a living imaging system (PerkinElmer, Hopkinton, USA). 24 and 72 h after intravenous injection, mice were euthanized to detect and quantify the fluorescence intensity of the tumor, heart, liver, spleen, lung, kidney, and genital system.

In Vivo Anti-Osteosarcoma Therapy: For the orthotopic osteosarcoma model, mice with tumors of ≈400 mm^3 were randomly divided into five groups with three mice in each group. PBS, Cu^{2+} ions, gossypol, Pre-CuGOS NPs, and CuGOS NPs (containing 20 mg mL^{-1} gossypol or 1.6 mg mL^{-1} $CuCl_2{\cdot}2H_2O$, 100 µL) were intravenously injected with the formulations every 3 days. The body weight and tumor volumes were monitored every 2 days. After various treatments for two weeks, mice were euthanized and dissected to analyze tumor progression. Orthotopic tumor and lung from each group were collected for photographing and weighing to understand the effect of each treatment on the progression of osteosarcoma. The histological analysis was used to detect intra-pulmonary tumor foci. The lung tissue was fixed in 4% paraformaldehyde for 24 h, embedded in paraffin, sectioned into 4 µm thickness, and stained with H&E. The stained slides were digitally scanned using a slide scanner (VS200, Olympus, Japan), and the resulting images were processed and exported using Case Viewer (3DHistech, Hungary).

The effectiveness of CuGOS NPs and doxorubicin were compared in the treatment of osteosarcoma in in situ osteosarcoma mouse model (average tumor volume ≈350 mm^3). Free doxorubicin (5 mg kg^{-1}, 100 µL) or CuGOS NPs (containing 20 mg mL^{-1} gossypol, 100 µL) were intravenously injected with the formulations every three days. Tumor volumes were monitored every two days. After treatment for two weeks, mice were euthanized, and orthotopic tumor were collected for photographing and weighing to understand the effect of each treatment on the progression of osteosarcoma.

In Vivo Biosafety: To better observe the effects of various treatment options on patients with osteosarcoma, tumor-bearing rather than healthy mice, were used as models. Mice were intravenously administered with CuGOS NPs (containing 20 mg mL^{-1} gossypol), and body weights were recorded every two days. At the endpoint (day 14), mice's blood and vital organs (heart, liver, spleen, lung, kidney, and genital system) were harvested. Blood biochemistry analysis, including ALT, AST, blood urea nitrogen (BUN), and creatinine (CRE), was tested by using an automatic biochemical analyzer (Chemray, Guangdong, China). These major organs were made into sections (4 µm) for histology analysis.

Statistical Analysis: All data were expressed as the mean ± SD and were analyzed with Prism 9.0 (Graph Prism Software, USA). The statistical difference between groups was analyzed by double-tailed student t test was employed to analyze the statistical difference between two groups. Two-tailed one-way ANOVA was employed to compare the difference between the means of multiple independent groups. Two-way ANOVA test followed by Sidak test for the comparison of multiple-group with two independent variables. Survival rate was analyzed by log-rank (Mantel-Cox) test. $P < 0.05$ was accepted as significant.[9,37]

Supporting Information

Supporting Information is available from the Wiley Online Library or from the author.

Acknowledgements

The authors would like to thank S. Wang at the Analytical & Testing Centre of Sichuan University for TEM characterization. This work was financially supported by the National Key R&D Program of China (J.G., Grant No. 2022YFA0912800), the National Natural Science Foundation of China (Y.O., Grant No. 82172682, Y.O., Grant No. 82373221, J.G., Grant No. 22178233, Q.K., Grant No. 82372447), the National Excellent Young Scientists Fund (J.G. Grant No. 00308054A1045), the Talents Program of Sichuan Province (J.G.), the Double First Class University Plan of Sichuan University (J.G.), the State Key Laboratory of Polymer Materials Engineering (J.G., Grant No. sklpme 2020-03-01), the Science and Technology Major Project of Tibetan Autonomous Region of China (Q.K., Grant No. XZ202201ZD0001G), the Science and Technology Project of Tibet Autonomous Region (Q.K., Grant No. XZ202303ZY0007G J.S., Grant No. XZ202301YD0027C), the Sichuan Tianfu Emei Project (J.G., Grant No. 2022-EC02-00073-CG), the Chongqing Science and Technology Commission (Y.O., Grant No. CSTB2023NSCQ-MSX0472), Chongqing Graduate Research Innovation Project (Q.F., Grant No. CYB23197), the 1·3·5 Project for Disciplines of Excellence, West China Hospital, Sichuan University (Q.K., Grant No. ZYJC21026), the First-class Discipline Construction Project of the First Affiliated Hospital of Chongqing Medical University (Q.F., Grant No. CYYY-BSYJSCXXM-202304).

Conflict of Interest

The authors declare no conflict of interest.

Author Contributions

J.G., Y.O., Q.K., and Q.F. designed the study. J.G., Y.O., and Y.H. supervised the study and experiments. Qingxin Fan conducted the experiment. Y.H.,

J.L., Q.L., Y.W., and Y.C. provided the technical support. Q.D., J.S., Q.K., Y.O., and J.G. provided funding and experimental platforms for the study. Y.H. managed the project and coordinated resources. Y.H., J.L., Q.L., Y.W., Y.C., and Qingxin Fan collected the data. J.L., Q.L., Y.C., and Qingxin Fan analyzed and interpreted the data. Qingxin Fan wrote the initial draft of the manuscript. Y.H., J.L., and Q.L. revised the initial manuscript draft. J.L., Q.L., Y.W., and Qingxin Fan were responsible for data visualization and formatting. J.G. and Y.O. were responsible for data archiving and storage. All authors discussed the results and commented on the manuscript. All authors have given approval to the final version of the manuscript.

Data Availability Statement

The data that support the findings of this study are available from the corresponding author upon reasonable request.

Keywords

drug discovery, genetic toxicity, large language model, metal-phenolic nanoplatform, osteosarcoma

Received: April 16, 2024
Revised: December 4, 2024
Published online:

[1] H. C. Beird, S. S. Bielack, A. M. Flanagan, J. Gill, D. Heymann, K. A. Janeway, J. A. Livingston, R. D. Roberts, S. J. Strauss, R. Gorlick, *Nat. Rev. Dis. Primers.* **2022**, *8*, 77.

[2] a) J. Gill, R. Gorlick, *Nat. Rev. Clin. Oncol.* **2021**, *18*, 609; b) C. Ratti, L. Botti, V. Cancila, S. Galvan, I. Torselli, C. Garofalo, M. C. Manara, L. Bongiovanni, C. F. Valenti, A. Burocchi, M. Parenza, B. Cappetti, S. Sangaletti, C. Tripodo, K. Scotlandi, M. P. Colombo, C. Chiodoni, *Clin. Cancer. Res.* **2017**, *23*, 5149.

[3] Y. Wang, M. Wang, Q. Wang, T. Wang, Z. Zhou, M. Mehling, T. Guo, H. Zou, X. Xiao, Y. He, X. Wang, O. J. Rojas, J. Guo, *Adv. Mater.* **2023**, *35*, 2301531.

[4] K. M. Tveter, E. Mezhibovsky, Y. Wu, D. E. Roopchand, *Pharmacol. Ther.* **2023**, *248*, 108457.

[5] a) P. Angulo, G. Kaushik, D. Subramaniam, P. Dandawate, K. Neville, K. Chastain, S. Anant, *J. Hematol Oncol.* **2017**, *10*, 10; b) X. L. He, G. D. Gong, M. Chen, H. J. Zhang, Y. J. Zhang, J. J. Richardson, W. Y. Chan, Y. X. He, J. L. Guo, *Angew. Chem. Int. Ed. Engl.* **2024**, *63*, 202314501; c) A. Khodaei, F. Jahanmard, H. R. Madaah Hosseini, R. Bagheri, A. Dabbagh, H. Weinans, S. Amin Yavari, *Bioact. Mater.* **2022**, *11*, 107; d) M. Motallebi, M. Bhia, H. F. Rajani, I. Bhia, H. Tabarraei, N. Mohammadkhani, M. Pereira-Silva, M. S. Kasaii, S. Nouri-Majd, A. L. Mueller, F. J. B. Veiga, A. C. Paiva-Santos, M. Shakibaei, *Life. Sci.* **2022**, *305*, 120752; e) Y. H. Qiao, Z. H. Wei, T. T. Qin, R. F. Song, Z. Q. Yu, Q. Yuan, J. Du, Q. B. Zeng, L. L. Zong, S. F. Duan, X. H. Pu, *Chinese. Chemical. Letters.* **2021**, *32*, 2877; f) W. Wang, D. Chen, K. Zhu, *J. Exp Clin. Cancer. Res.* **2018**, *37*, 37.

[6] a) F. Wong, E. J. Zheng, J. A. Valeri, N. M. Donghia, M. N. Anahtar, S. Omori, A. Li, A. Cubillos-Ruiz, A. Krishnan, W. Jin, A. L. Manson, J. Friedrichs, R. Helbig, B. Hajian, D. K. Fiejtek, F. F. Wagner, H. H. Soutter, A. M. Earl, J. M. Stokes, L. D. Renner, J. J. Collins, *Nature* **2023**, *626*, 177; b) Y. Zhang, C. Liu, M. Liu, T. Liu, H. Lin, C. B. Huang, L. Ning, *Brief. Bioinform.* **2023**, *25*, bbad467.

[7] a) Z. Zheng, A. H. Alawadhi, S. Chheda, S. E. Neumann, N. Rampal, S. Liu, H. L. Nguyen, Y. H. Lin, Z. Rong, J. I. Siepmann, L. Gagliardi, A. Anandkumar, C. Borgs, J. T. Chayes, O. M. Yaghi, *J. Am. Chem. Soc.* **2023**, *145*, 28284; b) Z. Zheng, Z. Rong, N. Rampal, C. Borgs, J. T. Chayes, O. M. Yaghi, *Angew. Chem. Int. Ed. Engl.* **2023**, *62*, 202311983.

[8] a) W. Chen, Y. Cai, Q. Fu, B. Chen, J. Guo, J. J. Chou, *Angew. Chem. Int. Ed. Engl.* **2019**, *58*, 9866; b) J. Guo, Y. Ping, H. Ejima, K. Alt, M. Meissner, J. J. Richardson, Y. Yan, K. Peter, D. von Elverfeldt, C. E. Hagemeyer, F. Caruso, *Angew. Chem. Int. Ed. Engl.* **2014**, *53*, 5546; c) J. Guo, M. Suástegui, K. K. Sakimoto, V. M. Moody, G. Xiao, D. G. Nocera, N. S. Joshi, *Science* **2018**, *362*, 813; d) J. Guo, B. L. Tardy, A. J. Christofferson, Y. Dai, J. J. Richardson, W. Zhu, M. Hu, Y. Ju, J. Cui, R. R. Dagastine, I. Yarovsky, F. Caruso, *Nat. Nanotechnol.* **2016**, *11*, 1105; e) J. Pan, G. Gong, Q. Wang, J. Shang, Y. He, C. Catania, D. Birnbaum, Y. Li, Z. Jia, Y. Zhang, N. S. Joshi, J. Guo, *Nat. Commun.* **2022**, *13*, 2117; f) X. Qiu, X. Wang, Y. He, J. Liang, K. Liang, B. L. Tardy, J. J. Richardson, M. Hu, H. Wu, Y. Zhang, O. J. Rojas, I. Manners, J. Guo, *Sci. Adv.* **2021**, *7*, eabh3482; g) Y. Zhang, J. Wang, Y. He, J. Pan, X. Jin, J. Shang, G. Gong, J. J. Richardson, I. Manners, J. Guo, *Angew. Chem. Int. Ed. Engl.* **2023**, *62*, 202303463; h) Z. Zhao, D. C. Pan, Q. M. Qi, J. Kim, N. Kapate, T. Sun, C. W. t. Shields, L. L. Wang, D. Wu, C. J. Kwon, W. He, J. Guo, S. Mitragotri, *Adv. Mater.* **2020**, *32*, 2003492; i) L. Chen, J. Min, F. Wang, *Signal Transduct Target Ther* **2022**, *7*, 378; j) S. R. Li, S. Y. Tao, Q. Li, C. Y. Hu, Z. J. Sun, *Biomaterials* **2025**, *313*, 122805; k) T. D. Rae, P. J. Schmidt, R. A. Pufahl, V. C. Culotta, T. V. O'Halloran, *Science* **1999**, *284*, 805.

[9] Q. Fan, J. Zuo, H. Tian, C. Huang, E. C. Nice, Z. Shi, Q. Kong, *J. Exp Clin. Cancer. Res.* **2022**, *41*, 162.

[10] H. Zhu, C. Huang, J. Di, Z. Chang, K. Li, S. Zhang, X. Li, D. Wu, *ACS Nano* **2023**, *17*, 12544.

[11] H. D. Williams, N. L. Trevaskis, S. A. Charman, R. M. Shanker, W. N. Charman, C. W. Pouton, C. J. Porter, *Pharmacol. Rev.* **2013**, *65*, 315.

[12] E. Ahire, S. Thakkar, M. Darshanwad, M. Misra, *Acta. Pharm. Sin B.* **2018**, *8*, 733.

[13] M. Wang, X. Yang, T. Huang, M. Wang, Y. He, G. Gong, Y. Zhang, X. Liao, X. Wang, Q. Yang, J. Guo, *ACS Nano* **2023**, *17*, 25136.

[14] X. Hou, D. Zhong, H. Chen, Z. Gu, Q. Gong, X. Ma, H. Zhang, H. Zhu, K. Luo, *Carbohydr. Polym.* **2022**, *292*, 119662.

[15] G. Gong, J. Pan, Y. He, J. Shang, X. Wang, Y. Zhang, G. Zhang, F. Wang, G. Zhao, J. Guo, *Theranostics* **2022**, *12*, 2028.

[16] K. Y. Choi, H. S. Han, E. S. Lee, J. M. Shin, B. D. Almquist, D. S. Lee, J. H. Park, *Adv. Mater.* **2019**, *31*, 1803549.

[17] L. W. C. Ho, C. K. W. Chan, R. Han, Y. F. Y. Lau, H. Li, Y. P. Ho, X. Zhuang, C. H. J. Choi, *ACS Nano* **2022**, *16*, 2032.

[18] a) S. A. Melville, J. Buros, A. R. Parrado, B. Vardarajan, M. W. Logue, L. Shen, S. L. Risacher, S. Kim, G. Jun, C. DeCarli, K. L. Lunetta, C. T. Baldwin, A. J. Saykin, L. A. Farrer, *Ann. Neurol.* **2012**, *72*, 65; b) T. P. Sharma, C. M. McDowell, Y. Liu, A. H. Wagner, D. Thole, B. P. Faga, R. J. Wordinger, T. A. Braun, A. F. Clark, *Mol. Neurodegener.* **2014**, *9*, 14.

[19] a) S. K. Holman, T. Morgan, G. Baujat, V. Cormier-Daire, T. J. Cho, M. Lees, J. Samanich, D. Tapon, H. D. Hove, A. Hing, R. Hennekam, S. P. Robertson, *Clin. Genet.* **2013**, *83*, 251; b) Y. Hou, F. Z. Li, *Eur. Rev. Med. Pharmacol. Sci.* **2021**, *25*, 7668.

[20] a) M. Brecqueville, J. Rey, R. Devillier, A. Guille, R. Gillet, J. Adélaide, V. Gelsi-Boyer, C. Arnoulet, M. Chaffanet, M. J. Mozziconacci, N. Vey, D. Birnbaum, A. Murati, *Haematologica* **2014**, *99*, 37; b) M. Fonódi, Z. Thalwieser, C. Csortos, A. Boratkó, *Int. J. Mol. Sci.* **2023**, *24*, 17360.

[21] a) N. Piri, Y. Q. Gao, M. Danciger, E. Mendoza, G. A. Fishman, D. B. Farber, *Ophthalmology* **2005**, *112*, 159; b) I. A. Viringipurampeer, X. Shan, K. Gregory-Evans, J. P. Zhang, Z. Mohammadi, C. Y. Gregory-Evans, *Cell. Death. Differ.* **2014**, *21*, 665.

[22] a) X. Ge, K. Zhang, A. Gribizis, A. S. Hamodi, A. M. Sabino, M. C. Crair, *Science* **2021**, *373*, eabd0830; b) P. Tarpey, S. Thomas, N. Sarvananthan, U. Mallya, S. Lisgo, C. J. Talbot, E. O. Roberts, M. Awan, M. Surendran, R. J. McLean, R. D. Reinecke, A. Langmann, S. Lindner, M. Koch, S. Jain, G. Woodruff, R. P. Gale, A. Bastawrous, C. Degg, K. Droutsas, I. Asproudis, A. A. Zubcov, C. Pieh, C. D. Veal,

R. D. Machado, O. C. Backhouse, L. Baumber, C. S. Constantinescu, M. C. Brodsky, D. G. Hunter, et al., *Nat. Genet.* **2006**, *38*, 1242.
[23] P. Wu, Y. Gao, S. Shen, Y. Xue, X. Liu, X. Ruan, L. Shao, Y. Liu, P. Wang, *Cell. Death. Dis.* **2019**, *10*, 536.
[24] Y. Matsumoto, J. Itou, F. Sato, M. Toi, *Cancer. Med.* **2018**, *7*, 454.
[25] M. Hassn Mesrati, S. E. Syafruddin, M. A. Mohtar, A. Syahir, *Biomolecules* **2021**, *11*, 1850.
[26] a) X. Wu, L. Qiu, H. Feng, H. Zhang, H. Yu, Y. Du, H. Wu, S. Zhu, Y. Ruan, H. Jiang, *Life. Sci.* **2022**, *293*, 120328; b) M. Zhao, Y. Zhang, L. Li, X. Liu, W. Zhou, C. Wang, Y. Tang, *Cancer. Cell. Int.* **2023**, *23*, 244.
[27] J. L. Lin, X. Fang, J. X. Li, Z. W. Chen, W. K. Wu, X. X. Guo, N. J. Liu, J. F. Huang, F. Y. Chen, L. J. Wang, B. Xu, C. Martin, X. Y. Chen, J. Q. Huang, *Nat. Plants.* **2023**, *9*, 605.
[28] a) K. Balakrishnan, W. G. Wierda, M. J. Keating, V. Gandhi, *Blood.* **2008**, *112*, 1971; b) J. Lian, D. Karnak, L. Xu, *Autophagy* **2010**, *6*, 1201.
[29] Y. Li, Y. Du, Y. Zhou, Q. Chen, Z. Luo, Y. Ren, X. Chen, G. Chen, *Cell. Commun. Signal.* **2023**, *21*, 327.
[30] a) C. Gridelli, A. Morabito, L. Cavanna, A. Luciani, P. Maione, L. Bonanno, V. Filipazzi, S. Leo, S. Cinieri, F. Ciardiello, M. A. Burgio, D. Bilancia, D. Cortinovis, F. Rosetti, R. Bianco, V. Gebbia, F. Artioli, R. Bordonaro, V. Fregoni, M. Mencoboni, F. Nelli, F. Riccardi, G. di Isernia, R. Costanzo, G. Rocco, G. Daniele, S. Signoriello, M. C. Piccirillo, C. Gallo, F. Perrone, *J. Clin. Oncol.* **2018**, *36*, 2585; b) T. T. T. Phan, N. V. Truong, W. G. Wu, Y. C. Su, T. S. Hsu, L. Y. Lin, *Cell. Death. Discov.* **2023**, *9*, 340.
[31] M. Berti, D. Cortez, M. Lopes, *Nat. Rev. Mol. Cell. Biol.* **2020**, *21*, 633.
[32] a) V. Queirós, U. M. Azeiteiro, A. Soares, R. Freitas, *J. Hazard. Mater.* **2021**, *412*, 125028; b) N. V. Volkova, B. Meier, V. González-Huici, S. Bertolini, S. Gonzalez, H. Vöhringer, F. Abascal, I. Martincorena, P. J. Campbell, A. Gartner, M. Gerstung, *Nat. Commun.* **2020**, *11*, 2169.
[33] E. Cybulla, A. Vindigni, *Nat. Rev. Cancer.* **2023**, *23*, 6.
[34] B. Yu, Y. Wang, T. Bing, Y. Tang, J. Huang, H. Xiao, C. Liu, Y. Yu, *Adv. Mater.* **2023**, *36*, 2310456.
[35] S. S. Bielack, B. Kempf-Bielack, G. Delling, G. U. Exner, S. Flege, K. Helmke, R. Kotz, M. Salzer-Kuntschik, M. Werner, W. Winkelmann, A. Zoubek, H. Jürgens, K. Winkler, *J. Clin. Oncol.* **2023**, *41*, 4323.
[36] G. He, J. J. Nie, X. Liu, Z. Ding, P. Luo, Y. Liu, B. W. Zhang, R. Wang, X. Liu, Y. Hai, D. F. Chen, *Bioact. Mater.* **2023**, *19*, 690.
[37] M. Yang, Y. Zhang, F. Mou, C. Cao, L. Yu, Z. Li, J. Guan, *Sci. Adv.* **2023**, *9*, eadk7251.